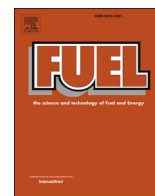


Combustion characterization of hybrid methane-hydrogen gas in domestic swirl stoves.

LIU, X., ZHU, G., ASIM, T. and MISHRA, R.

2022

© 2022 The Author(s).



Full Length Article

Combustion characterization of hybrid methane-hydrogen gas in domestic swirl stoves

Xiaozhou Liu^a, Guangyu Zhu^a, Taimoor Asim^{b,*}, Rakesh Mishra^c

^a Guangdong University of Technology, China

^b School of Engineering, Robert Gordon University, AB10 7GJ, UK

^c School of Computing & Engineering, University of Huddersfield, HD1 3DH, UK



ARTICLE INFO

Keywords:

Swirl gas stoves
Hybrid methane-hydrogen mixture
Hot-state tests
Numerical simulations
CO emission

ABSTRACT

Combustion of hybrid natural gas (methane) and hydrogen mixture in domestic swirl stoves has been characterized using hot-state experiments and numerical analysis. The detailed combustion mechanism of methane and hydrogen (GRI-Mech 3.0) has been simplified to obtain reduced number of chemical reactions involved (82 % reduction). The novel simplified combustion mechanism developed has been used to obtain combustion characteristics of hybrid methane-hydrogen mixture. The difference between the calculations from the detailed and the simplified mechanisms has been found to be <1 %. A numerical model, based on the simplified combustion model, is developed, rigorously tested and validated against hot-state tests. The results depict that the maximum difference in combustion zone's average temperature is <13 %. The investigations have then been extended to hybrid methane-hydrogen mixtures with varying volume fraction of hydrogen. The results show that for a mixture containing 15 % hydrogen, the release of CO due to combustion reduces by 25 %, while the combustion zone's average temperature reduces by 6.7 %. The numerical results and hot-state tests both confirm that the temperature remains stable when hybrid methane-hydrogen mixture is used in domestic swirl gas stoves, demonstrating its effectiveness in cooking processes.

1. Introduction

The Paris Agreement emphasis on the development of low-carbon and zero-carbon solutions to achieve carbon neutrality [1]. As it is a legally binding international treaty, countries all over the world are concentrating their efforts to reduce dependence on carbon-based fuels, which can have significant impact on reducing environmental pollution. The exponential increase in the use of coal in China from 2000 to 2010 has become stable since 2015 as it looks to gradually replace coal with natural gas as the primary source of energy [2]. The second most energy consuming sector in China is domestic (after industrial) where natural gas is becoming increasingly popular for heating and cooking purposes. For cooking, the majority households use swirl gas stoves, with CO being the main pollutant emitted [3]. If China has to fulfil its commitment to make non-fossil fuel energy only 20 % of its total energy supply, it will have to look towards carbon-zero fuels, such as Hydrogen, to be adopted as the primary fuel for domestic applications. At present, adding hydrogen to natural gas is an effective means to reduce hazardous CO emissions and improve the thermal efficiency of gas stoves. An

important question arises here that how much hydrogen can be added to methane in domestic stoves.

Haeseldonckx et al. [4], through calculating the Warburg number, concluded that when <17 % of hydrogen is mixed in the natural gas pipeline (in Belgium), the hybrid gas can be safely used in domestic and commercial stoves. Hu et al. [5] designed a constant volume combustion chamber system and analysed it through the use of schlieren high-speed photography. Experimental results show that when the hydrogen concentration is <60 %, the combustion state is dominated by methane combustion. A transitional state has been observed for hydrogen concentration between 60 % and 80 %. When hydrogen concentration is >80 %, methane inhibits combustion of hydrogen. Donohoe et al. [6] conducted experiments to measure ignition delay time in shock tubes and fast compressors. Chemkin software was used to simulate the experimental data, while the results were consistent with the experiments. Experimental results show that the ignition delay time decreases with the increase of temperature, pressure, hydrogen mixing ratio and the increase of long-chain hydrocarbons. Ahmed et al. [7] conducted experiments and numerical simulations to explore the effects of

* Corresponding author.

E-mail address: t.asim@rgu.ac.uk (T. Asim).

<https://doi.org/10.1016/j.fuel.2022.126413>

Received 1 May 2022; Received in revised form 28 September 2022; Accepted 16 October 2022

Available online 30 October 2022

0016-2361/© 2022 The Author(s). Published by Elsevier Ltd. This is an open access article under the CC BY license (<http://creativecommons.org/licenses/by/4.0/>).

hydrogen doping on the chemical structure of methane flames under sooting conditions. The results show that the addition of hydrogen affects the chemical microstructure of methane flame while keeping the C/O ratio and the cold gas flow rate constant. Ying et al. [8] studied the detailed chemical effects of hydrogen as a fuel additive on the laminar premixed methane / air flame. The dilution and thermal effects lead to the addition of hydrogen in the flame, which reduces the molar fraction of C_2H_2 and CH_2CO , and also reduce the formation of oxygen-containing pollutants CH_2O and CH_3CHO .

As the combustion characteristics of hydrogen are substantially different from those of natural gas (methane), extensive investigations need to be carried out in order to better understand the complex combustion characteristics of a mixture of methane and hydrogen. With a perspective of potential use of hybrid methane-hydrogen mixture in domestic gas stoves, Luo et al. [9] studied the combustion safety and emission performance of the fuel composed of hydrogen and natural gas on domestic gas appliances. The experimental results show that the flame stability and flue gas emissions meet the requirements of national standards. Zhao et al. [10] studied the combustion characteristics of fuel gas under different hydrogen doping concentrations. The results show that although doping hydrogen effectively reduce the emission of pollutants, when the volume of hydrogen doping in fuel gas is 20 %, backfire will occur in domestic gas stoves. Jiang et al. [11] used numerical simulations to study the effects of primary air coefficient, fire hole cone angle and pot support height on the thermal efficiency of domestic gas stoves. Although the optimal influence factor combination under orthogonal experimental conditions was obtained, but it was not experimentally verified. Chen et al. [12] studied the influence of different primary air coefficient on the flame shape of high-power domestic gas stove under the same power through numerical simulation. Pashchenko [13] conducted a detailed study of hydrogen-rich combustion in a swirling flame using Computational Fluid Dynamics (CFD) and found that an increase in the hydrogen mole fraction leads to an increase in the combustion temperature. Hydrogen-rich fuel blends produce less nitrogen oxides than pure methane. Sun et al. [14] studied the effect of mixing hydrogen in natural gas at a volume ratio of 0–20 % on the performance of domestic gas appliances. The results show that when the volume of mixed hydrogen is 25 %, backfire will occur in the domestic gas water heater. Jones et al. [15] analyzed the feasibility of mixing hydrogen based on the natural gas characteristics and terminal equipment in the UK. When the hydrogen content increases, the parameter area where backfire may occur is expanded. By adjusting the shape and angle of the burner, the swirl flame can be formed to improve the flame stability. Zhao et al. [16] evaluated the interchangeability of hydrogen and natural gas for residential commercial oven burners and concluded that addition of hydrogen will reduce the ignition time. It has been reported that the ignition backfire limit is a state with 25 % hydrogen concentration. Compared with pure natural gas, adding 10 % hydrogen increases the burner temperature by 63 %. Moreover, addition of hydrogen does not significantly change NO_x emission level, but reduces the CO emission.

As hydrogen is combustible and explosive, at present, researchers around the world generally use numerical methods to investigate the combustion performance of hydrogen doped natural gas. The detailed mechanism used in this study is the GRI-MECH 3.0 [17] combustion model, which is widely used in the study of methane and hydrogen combustion characteristics. The GRI-Mech 3.0 reaction mechanism contains 53 component and 325 reactions, however, the computational power required to carry out these calculations is prohibitive, often requiring the use of supercomputer facilities. If a simplified version of the detailed combustion model is developed, it will significantly aid in reducing the computational requirements, but the accuracy of the simplified model will need to be verified against the detailed model. Sensitivity Analysis (SA) is often used in the simplification of combustion mechanism and has been widely used in recent years. Hou et al. [18] developed a 10-step 12-component simplified combustion

mechanism suitable for methane rocket engine through sensitivity analysis. This mechanism is consistent with the detailed mechanism for the prediction of equilibrium temperature and main concentration. Jiang et al. [19] simplified the 58-step elementary reaction through sensitivity analysis for the combustion characteristics of piston engine. The simplified model can accurately predict the premixed combustion phenomenon in the engine. Wang et al. [20] simplified the model of 15-components for Perfectly Stirred Reactor (PSR) model by combining temperature sensitivity and production rate, which is suitable for the combustion of phenolic resin pyrolysis products in air under supersonic conditions, in which the pyrolysis gas includes H_2O , CH_4 , CO , H_2 , CO_2 etc. Ruan et al. [21] developed the full mixed-flow reaction model through the PSR model. Through the reaction path, it was found that the main NCO free radicals and N_2O free radicals in the NO compound reduction reaction were significantly affected by the temperature. Increasing the temperature was conducive to the generation and consumption of NCO and N_2O free radicals, which is beneficial to the reaction.

The Direct Relation Graph (DRG) method [22] has also been widely used in combustion mechanism simplification. Fany et al. [23] simplified the detailed mechanism of Dodecane combustion by using DRG and Calculation Singular Value Perturbation method. The calculation results show that the simplified mechanism can reproduce the simulation results of Dodecane in the aspects of ignition delay time, flameout and species concentration distribution under high temperature combustion condition. Lu et al. [24] and Poon et al. [25] carried out further research work and simplified the combustion mechanism by using the two-step DRG method and observed that the calculation efficiency of this mechanism significantly improved. Monnier et al. [26] simplified the RAMEC mechanism through the direct relationship graph with error propagation (DEGEP) [27] and verified the simplified mechanism through the one-dimensional premixed flame model. Results show that temperature difference between the simplified mechanism and the detailed mechanism is 4 %, and the calculation speed is increased by 8 times compared to the detailed mechanism. Simplified mechanism can accurately calculate the combustion results of methane and oxygen under high pressure conditions. Tang et al. [28] simplified the mechanism after the coupling of kee-58 mechanism and Aramco Mech 1.3 according to the directed relationship graph method (DRGEP) [29] combining sensitivity analysis and error analysis for the combustion of methane and dimethyl ether at the micro scale. Results of simulation calculation based on simplified mechanism are the same as the flame shape and flameout limit in the experiment. Hu et al. [30] simplified the USC mech II mechanism under the high-pressure oxygen enriched combustion condition through the directed relationship graph method and time scale reduction analysis. Difference between the high-pressure oxygen enriched combustion flame calculated by the simplified mechanism and the detailed mechanism is within 10 %. Li et al. [31] simplified the detailed mechanism based on AramcoMech 2.0 mechanism through the directed relationship graph method for the mixed combustion of ammonia, hydrogen and methane. Simplified mechanism has been simulated in the coaxial common flow burner with turbulent non-premixed jet flame. Results are in close agreement with the detailed mechanism, and the calculation time is only 20 % of the detailed mechanism.

Based on the GRI-Mech 3.0 mechanism, the simplified methane-hydrogen combustion mechanism with 26 components and 143 reactions was obtained by Gimeno-Escobedo et al [17] using Chemkin software. It is verified by the calculation results in a zero-dimensional homogeneous reactor and one-dimensional free flame propagation, which shows that the error is kept within a reasonable range. The simplified mechanism reduces the number of chemical reactions by 56 % compared to the conventional detailed mechanism. In the present study, a simplified combustion mechanism for hybrid methane-hydrogen mixture to be used in domestic gas stoves has been developed using Sensitivity Analysis (SA) and Direct Relationship Graph (DRG) methods.

The novel mechanism reduces the number of chemical reactions of the detailed mechanism by 82 %, thus decreasing the computational power required significantly. The simplified mechanism is then implemented in the numerical solver for the combustion analysis. The numerical predictions have been validated against experimental results through hot-state tests. The effectiveness of the simplified combustion model is compared with the detailed model through comparative analysis, providing a reference basis for the wide application of hybrid methane-hydrogen gas in domestic swirl gas stoves.

2. Development of the simplified combustion mechanism

The simplified combustion mechanism model developed in the present study is based on the Perfectly Stirred Reactor (PSR) model in CHEMKIN, which is a software widely used for solving complex chemical kinetics in a wide variety of combustion applications [32]. PSR [33] is a Fortran program that predicts the steady-state temperature and species composition in a PSR. The reactor in this model is characterized by a reactor volume, residence time or mass flow rate, heat loss, reaction temperature and the mixture composition. The model accounts for finite-rate elementary chemical reactions. The governing equations are a system of nonlinear algebraic equations. The program solves these equations using a hybrid Newton/time-integration method. The program runs in conjunction with the CHEMKIN package, which handles the chemical reaction mechanism. The PSR model has been used to study combustion mechanism of fuel in this study as the combustion condition described by this model is similar to that of a gas stove. The available chemical reaction kinetic model for combustion modelling of methane and hydrogen with oxygen has been simplified using Sensitivity Analysis (SA), Direct Relation Graph (DRG) and DRG with Error Propagation (DRGEP) techniques. The simplified chemical reaction kinetic model obtained has then been analyzed in detail.

2.1. Temperature sensitivity analysis

The detailed chemical reaction mechanism (GRI-Mech 3.0) is simplified using sensitivity analysis method, and the temperature sensitivity analysis of overall and key components has been carried out for the full reaction process of methane and hydrogen mixture in air. The overall sensitivity analysis result is shown in Fig. 1. It can be seen from that the combustion reaction is mainly promoted by $H + O_2 \rightleftharpoons O + OH$ (R13). This reaction converts O_2 into the concentration of O radical and accelerates combustion. The reactions of negative temperature sensitivity coefficient are mainly $H + CH_4 \rightleftharpoons CH_3 + H_2$ (R24) and $OH + CH_4 \rightleftharpoons CH_3 + H_2O$ (R30). In the actual combustion process, R24 and R30 consume H radical and OH radical, which slows down the

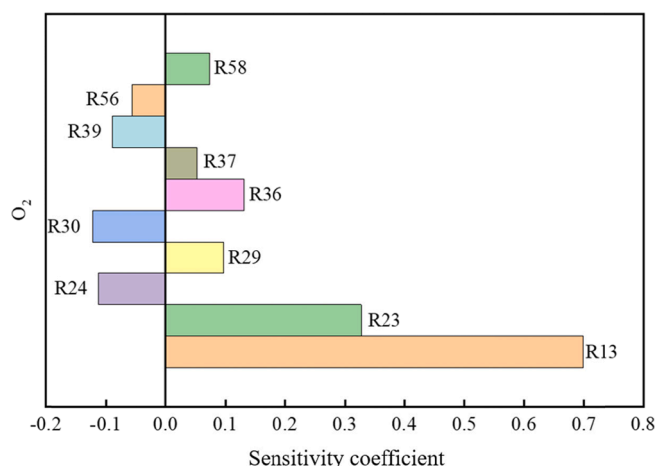


Fig. 1. Overall temperature sensitivity analysis.

oxidation rate. It should be noted that the time when the sensitivity coefficient of each elementary reaction reaches the peak is different, and the peak point of each reaction is selected in the subsequent analysis.

The equations included in the overall temperature sensitivity are summarized in Table 1. It is evident that H_2 , O_2 , CH_4 , CH_3 and OH are the key reaction components. The sensitivity analysis has been carried out to analyze the temperature sensitivity of all the key components. Further simplification of the whole reaction process is achieved by removing the elementary reaction with small sensitivity coefficient and retaining the elementary reaction with large sensitivity coefficient.

The sensitivity analysis results of the key components are shown in Fig. 2. It can be seen that there is a certain difference between the temperature sensitivity of the base component and the temperature sensitivity of the total reaction. However, the reactions with higher absolute value of temperature sensitivity are the same for the reactions R13, R24, R23, R30 and R36. These reactions contain important elementary units, which are H, O, O_2 , OH, CH_3 , CH_4 , H_2 and H_2O .

2.2. Direct relation graph

The elementary units identified through sensitivity analysis are further simplified using Direct Relation Graph (DRG) method [22]. This method can effectively simplify the secondary components and elementary reactions in the detailed mechanism, but also have some shortcomings. DRG ignores the weakening of the correlation between components when propagating along the path. In order to reduce the error caused by the simplification of one-step DRG, this study adopts the method of DRG combined with Error Propagation (EP), thus resulting in DRGEP method [27]. In the simplification process, the key elementary components (H, O, O_2 , OH, CH_3 , CH_4 , H_2 and H_2O) and reaction products (CO and CO_2) obtained from the sensitivity analysis are searched as the initial component set, and the obtained component set is coupled with the important components of the initial detailed mechanism. The calculated results of different sample points are then combined to obtain the final reaction component set. The reaction equation with the components contained in the set is regarded as an important reaction, and its equation is retained to construct a simplified mechanism.

In order to achieve this, the combustion conditions of the hybrid methane-hydrogen gas mixture are simplified and PSR model is implemented. The calculation condition of this PSR model is set as follows: the initial reaction temperature is $T = 1800$ K, the pressure is $P = 1$ atm and the residence time is $t = 0.01$ s. The values of these parameters are derived from the data of the gas stove in normal operation. Because methane has a very high calorific value, its maximum combustion temperature reaches as high as 1800 K. Furthermore, since the reaction speed of methane is extremely fast, the reaction time is taken as 0.01 s in this paper. P is defined as 1 atm, which means that the combustion experiment is carried out under atmospheric conditions. The volume of the reactor is 282 cm^3 . Ignoring the heat loss, the mole fractions of CH_4 , H_2 and O_2 are 0.109, 0.05 and 0.183 respectively, and the equivalence ratio is 1.6. The absolute error and relative error in the simplification process are set to 10^{-5} and 10 % respectively. The mechanism simplified by DRG method is 72 steps reaction of 19 components. DRGEP method is

Table 1
Key reaction equations.

R13	$H + O_2 \rightleftharpoons O + OH$
R23	$H + CH_3(+M) \rightleftharpoons CH_4(+M)$
R24	$H + CH_4 \rightleftharpoons CH_3 + H_2$
R29	$OH + CH_3 \rightleftharpoons CH_2(S) + H_2O$
R30	$OH + CH_4 \rightleftharpoons CH_3 + H_2O$
R36	$CH_2 + CH_4 \rightleftharpoons 2CH_3$
R37	$CH_2(S) + N_2 \rightleftharpoons CH_2 + N_2$
R39	$CH_2(S) + O_2 \rightleftharpoons CO + H_2O$
R56	$O + CH_3 \rightleftharpoons H + H_2 + CO$
R58	$CH_2 + O_2 \rightleftharpoons 2H + CO_2$

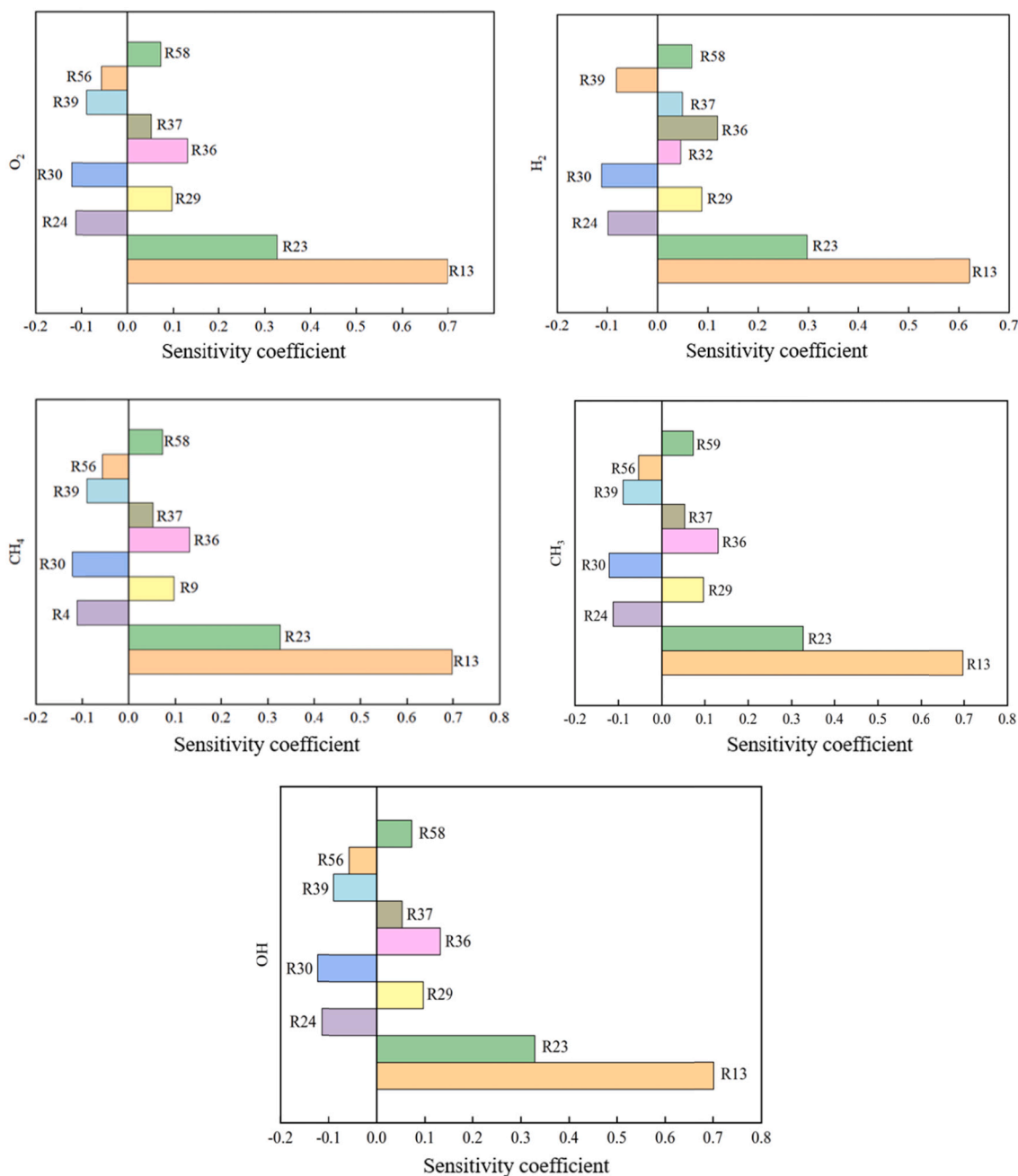


Fig. 2. Sensitivity analysis of O_2 , H_2 , CH_4 , CH_3 and OH .

used to continue the simplification. The original 53 component and 325 steps reaction model is simplified to 17 component and 58 steps reactions model, which significantly reduces the calculation workload. The complete simplified reaction model is provided in the appendix.

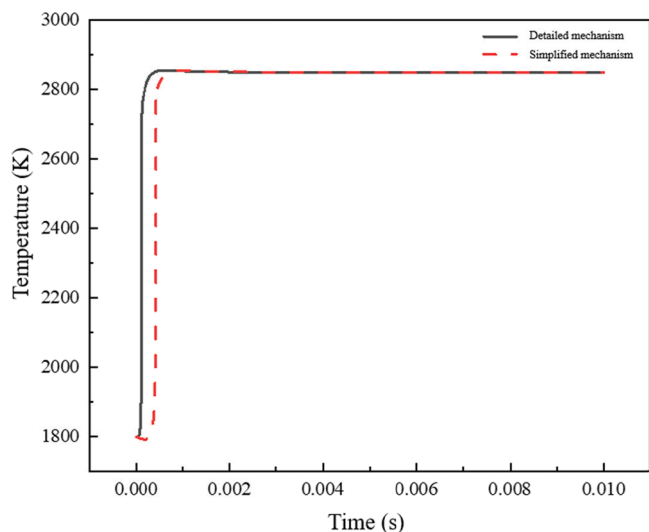
In order to verify the accuracy of the simplified model developed, the results calculated using this model are compared against the results obtained from the detailed model. The comparative analysis depict that the simplified mechanism is applicable to the calculation of pure methane and methane-hydrogen doping conditions, as shown in Fig. 3. It can be seen that by deleting some components, the generated substances in some reactions reduce after simplification, and the chain activation reaction lags behind, resulting in the change of position of the flame. With the passage of time, when the combustion is in a stable state, the error between the two mechanisms is no > 1 %, which proves the validity of the simplified mechanism.

3. Numerical combustion analysis of methane in a swirl gas stove

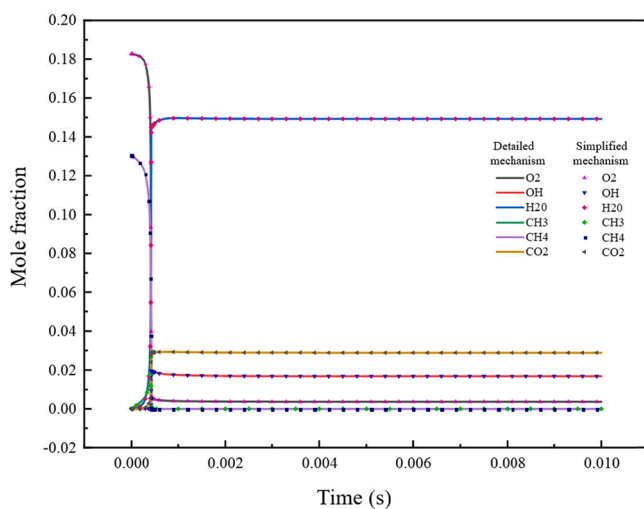
The simplified mechanism developed in this study is applicable to the combustion of both pure methane and hybrid methane-hydrogen mixture. This section provides details of combustion of methane only, while the combustion characteristics of hybrid methane-hydrogen mixture are presented in Section 4. The experimental validation of the numerical results has been carried out for the combustion of methane and hybrid methane-hydrogen mixture (with 15 % Hydrogen).

3.1. Geometric model of the swirl gas stove

A typical domestic swirl gas stove is shown in Fig. 4. It consists of two burner rings and a heat-resistant quartz plate on top. These gas stoves are widely used in China in the domestic sector for cooking purposes.



(a)



(b)

Fig. 3. Comparison of (a) temperature and (b) mole fraction of the key components from the simplified and the detailed mechanisms.



Fig. 4. Swirl gas stove.

Luo et al. [34] have reported that swirling enhances the supplement and mixing function of secondary air and is conducive to more complete combustion, thus making swirl gas stoves more efficient than straight gas stoves.

Based on the swirl gas stove shown in Fig. 4, a geometric model has been created in ANSYS® [35], as shown in Fig. 5. The stove comprises of two parts i.e. the burner and the quartz plate on top of the burner. The burner has two rings i.e. the outer ring and the inner ring; each ring has its own inlet. The dimensions of the different geometric features of the model are summarized in Table 2.

Since the fuel is evenly distributed after entering the premixing chamber, the model is axially symmetrical and thus, 1/6th of the model has been used for further modelling, as shown in Fig. 6.

3.2. Spatial discretization of swirl gas Stove's flow domain

The flow domain of the swirl gas stove is a cylinder with a diameter of 500 mm and a height of 200 mm. An unstructured mesh comprising of polyhedral elements has been generated in the flow domain [36]. The density of the mesh elements in the combustion zone i.e. in the vicinity of the fire holes is kept relatively higher compared to rest of the flow domain. The meshed flow domain is shown in Fig. 7(a). In order to ascertain the independence of numerical predictions from the density of mesh elements in the flow domain, a number of meshes have been generated. The parameter that has been chosen for mesh independence tests is the flow velocity at the exit of fire holes. It can be seen in Fig. 7(b) that as the number of mesh elements increases from $\sim 1 \times 10^5$ to $\sim 2 \times 10^5$, the flow velocity at the exit of fire holes decreases from 2.84 m/s to 2.70 m/s (4.9% decrease). On further increasing the mesh density to $\sim 3 \times 10^5$, the flow velocity remains almost the same. Thus, the mesh with $\sim 2 \times 10^5$ elements has been chosen for numerical analysis in the present study.

3.3. Specifications of the boundary conditions

The boundary types specified to the swirl gas stove model are shown in Fig. 8. It can be seen that top surface of the model (A) is the outlet of the combustion products and has been modelled as a pressure outlet. The circumferential surface (B) is the secondary air inlet and has been modelled as a pressure inlet boundary. Surfaces C₁ and C₂ are the inlets of inner and outer rings respectively and thus, have been modelled as velocity inlets. Surface D is the heat-resistant quartz plate which has been modelled as a solid wall with thermal coupling between the solid and fluid regimes. Surface F is the periodic boundary (due to symmetry) and surface E has been specified as the adiabatic wall. Since the upper half of the heat-resistant quartz plate is the flue gas outlet, the mesh density is higher in this region (see Fig. 7).

The boundary conditions specified to the numerical model of the swirl gas stove have been summarized in Table 3. The calculated load of the gas stove is 3.8 kW and the equivalence ratio is ~ 1.6 .

3.4. Combustion modelling

The Finite Rate Model (FRM) has been employed in the present study as the combustion model. In order to avoid errors caused by frequency factor and activation energy in the reaction rate, a double precision solver is used in the calculation process. The governing equation of combustion reaction is:

$$R_i = M_{w,i} \sum_{r=1}^{N_R} R_{i,r} \quad (1)$$

where $M_{w,i}$ is the molar molecular weight of component i and $R_{i,r}$ is the Arrhenius molar rate of generation/decomposition of component i . When the reaction proceeds in the forward direction, the governing equation of the forward reaction constant $k_{f,r}$ is:

$$k_{f,r} = A_r T^{\beta_r} e^{-E_r/RT} \quad (2)$$

where A_r is the frequency factor, β_r is temperature index

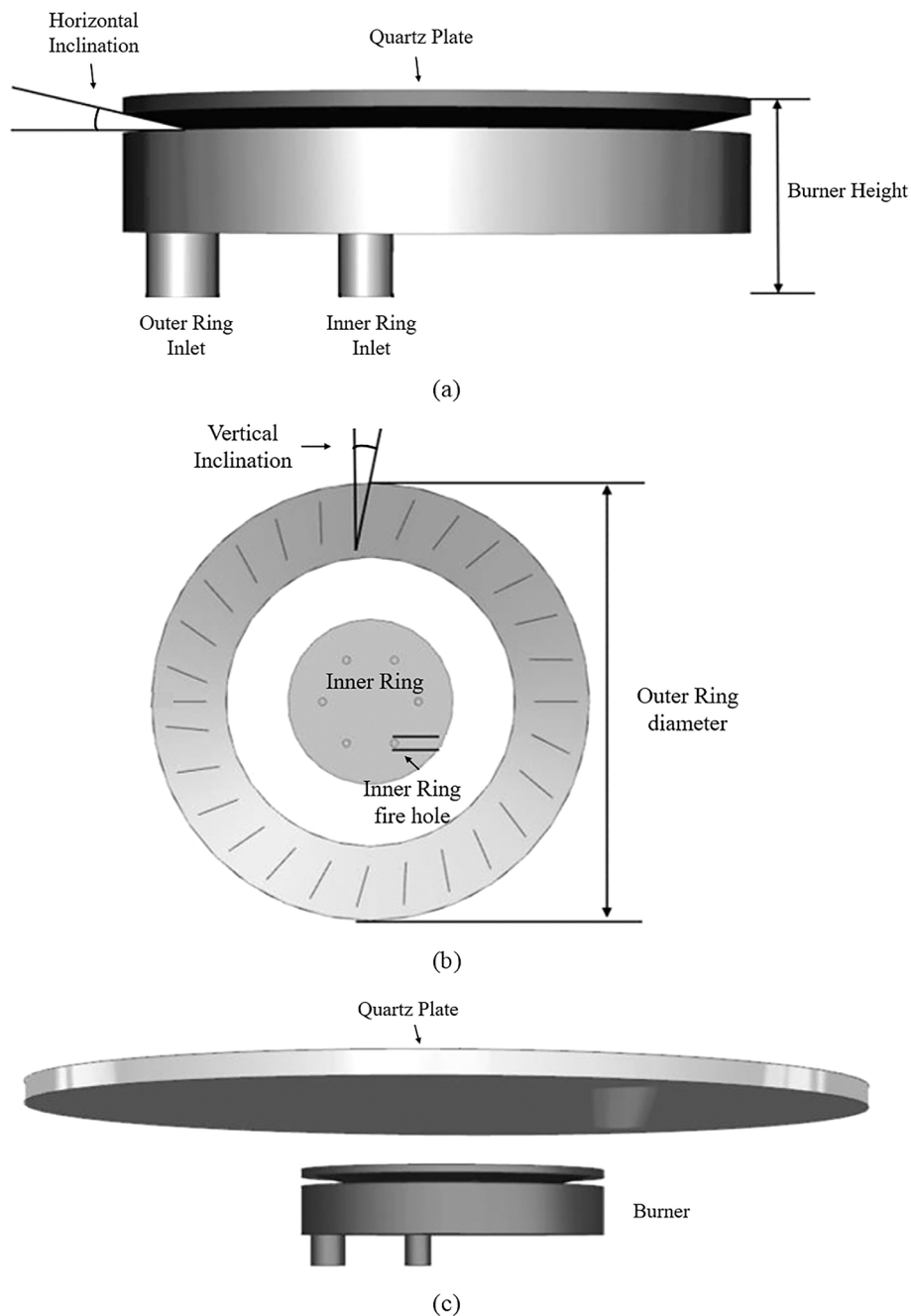


Fig. 5. Geometric model of the swirl gas stove a) burner; b) rings of the burner; c) complete model.

Table 2
Geometric details of the swirl gas stove model.

Feature	Dimension
Outer Ring diameter	120 mm
Outer Ring Inlet	13.5 mm
Inner Ring diameter	10.3 mm
Inner Ring Inlet	11.9 mm × 0.1 mm
Inner Ring Fire Holes diameter	1.95 mm
Burner Height	37 mm
Burner's Horizontal Inclination	14°
Burner's Vertical Inclination	11.7°
Quartz Plate's diameter	320 mm
Quartz Plate's thickness	8 mm

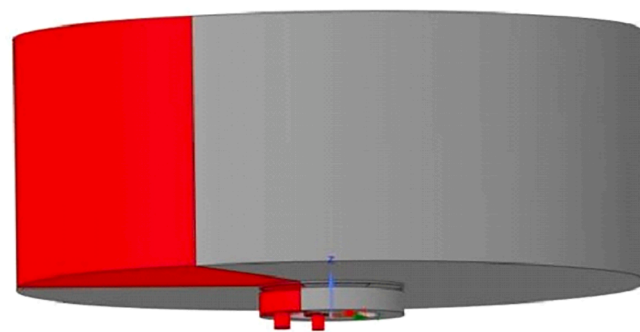
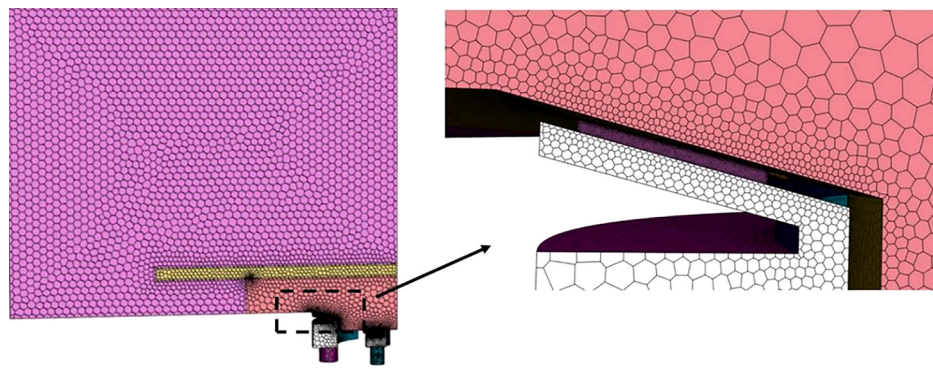
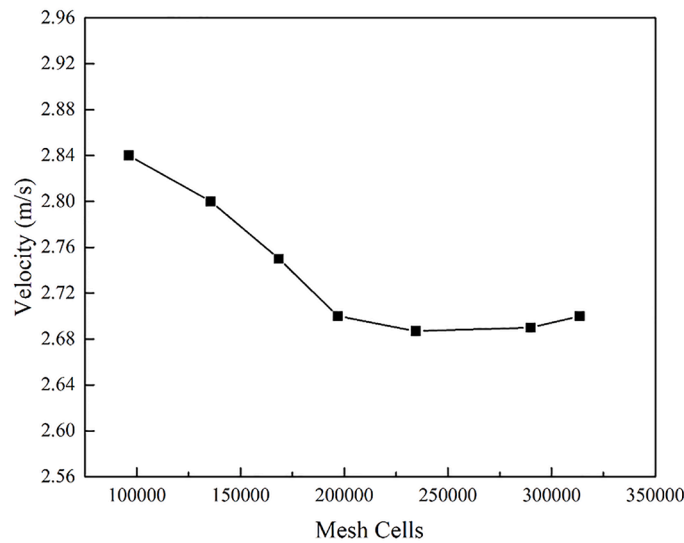


Fig. 6. 1/6th model of the swirl gas stove (highlighted).



(a)



(b)

Fig. 7. (a) Meshing of the swirl gas stove's flow domain (b) Mesh independence test results.

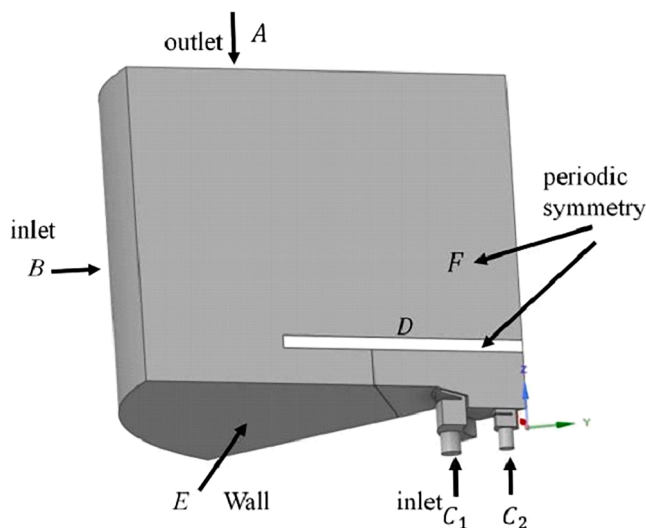


Fig. 8. Boundary conditions for the swirl gas stove model.

(dimensionless), E_r is the activation energy in the reaction (J/kmol) and R is the general gas constant. When the reaction proceeds in reverse direction, the governing equation of the reverse reaction constant is:

Table 3
Boundary conditions.

Boundary	Velocity (m/s)	Hydraulic diameter (cm)	Mole fraction	Temperature (K)
Inner ring inlet	0.15	0.92	CH ₄ :0.159, O ₂ :0.18	315
Outer ring inlet	0.25	1.25	CH ₄ :0.159, O ₂ :0.18	315
Air inlet	-	80	O ₂ :0.2181	300
Air outlet	-	50.8	-	-

$$k_{b,r} = \frac{k_{f,r}}{K_r} \quad (3)$$

where K_r is the equilibrium constant of reaction r . The chemical reaction mechanism (GRI-Mech 3.0), which is applicable to both pure methane and hydrogen doped methane, has been simplified above, and this model has been used for numerical investigations and experimental validation in this study.

3D Navier-Stokes equations have been iteratively solved for steady flow of combustion gases in the flow domain. Turbulence in the flow has been modelled using 2-equation Shear Stress Transport $k-\omega$ model [37]. The simplified combustion mechanism is incorporated into the component transport model. The SIMPLE algorithm is used to couple the flow velocity and pressure, while the momentum and energy equations have

been discretized using second-order upwind method.

3.5. Temperature distribution on the quartz plate

Thermal variations on the top surface of the heat-resistant quartz plate have been obtained through numerical simulations, which have then been validated against the experimental data obtained. The aim here is to ascertain the appropriateness of the numerical modelling approach used, which can then be extended to carry out the numerical combustion modelling of hybrid methane-hydrogen mixture in the same swirl gas stove. The thermal variations shown in Fig. 9 indicate that the temperature in middle region of the quartz plate is significantly higher compared to the temperature along the periphery of the quartz plate. Thus, thermal gradient in the radial direction of the quartz plate is visible. Looking closely at Fig. 5(c), it is evident that the high temperature on the quartz plate is due to the burner rings directly under this region.

3.6. Experimental validation of methane combustion

The thermal and velocity fields associated with domestic swirl gas stoves are very difficult to measure directly as the temperature is quite high. Therefore, in the present study, the method adopted by Vijaykumar Hindsageri [38] has been used for thermal characterization of the swirl gas stove. During the experiments, thermal image of the heat-resistant quartz plate has been obtained after stable combustion has been achieved. Thermal stability is gauged through the stability in the temperature readings, with variations not exceeding 5 °C. The thermal image has been captured using an infrared imager FLUKE TiX640, which has a measurement range of -40 °C to 1200 °C, and a measurement error of not more than ±1.5 °C.

Fig. 10 depicts the temperature variations on the top surface of the heat-resistant quartz plate. As observed in case of numerical thermal analysis of the plate, it can be seen that the temperature is considerably higher in the middle region of the plate, while the temperature is lower in the peripheral regions. Moreover, it is observed that the temperature profile measured experimentally on the quartz plate is quite non-uniform in comparison with the numerically predicted temperature profile. The primary contributor to this difference is the geometrical differences between the two environments; the experiments are performed in an open space while the numerical modelling is carried out in a small cylindrical domain. Experimental investigations carried out by Zheng [39] indicate that the heat loss from the flue gas accounts for ~18 % of the total heat loss. It can be seen in Fig. 10 that at the edge of the quartz plate, the flue gas begins to surge upward, resulting in significant

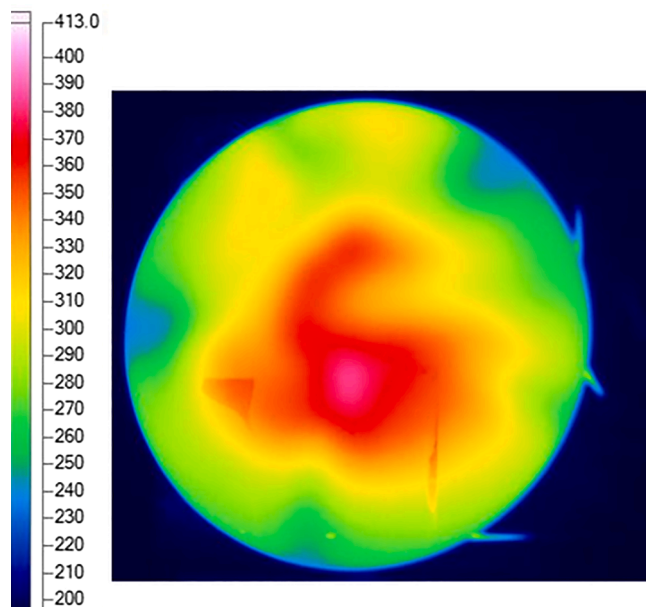


Fig. 10. Thermal image of the heat-resistant quartz plate (°C).

amount of heat loss, which makes the temperature field uneven. There is a need to carry out extensive quantitative analysis to highlight the differences between the two methodologies employed in this study. It should however be noted that the scaling used in Figs. 9 and 10 are different; the maximum scale value is the same but the minimum scale value is different.

As mentioned earlier, a detailed quantitative analysis is required in order to evaluate the differences between the experimental and the numerical results. This has been carried out in this study using the equal section method proposed by Jin et al. [40]. Average temperature values are computed on a series of circular paths on the top surface of the heat-resistant quartz plate, as shown in Fig. 11. The radii of these paths are 75 mm, 100 mm, 125 mm and 150 mm respectively.

The average temperature values on these circular paths have been summarized in Table 4. It can be seen that as the radius of the circular paths increase (radially outwards on the quartz plate), the difference between the numerically predicted and experimentally recorded average temperature values increases. It can be seen from that the average temperature predicted by the numerical solver at the periphery of the heat-resistant quartz plate (150 mm) is ~13 % lower than

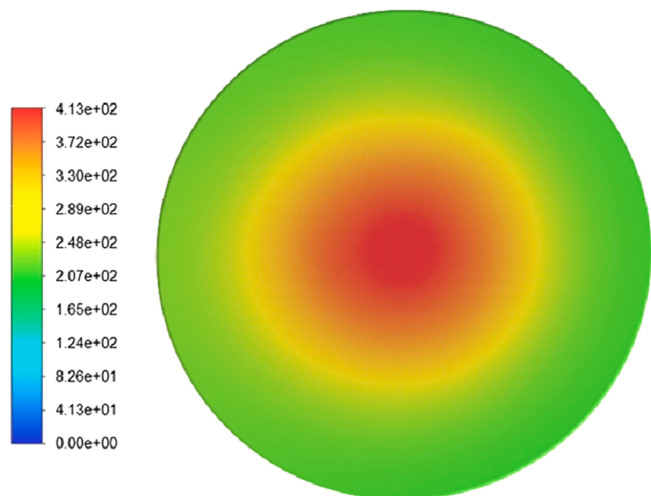


Fig. 9. Static temperature (in °C) variations on the heat-resistant quartz plate.

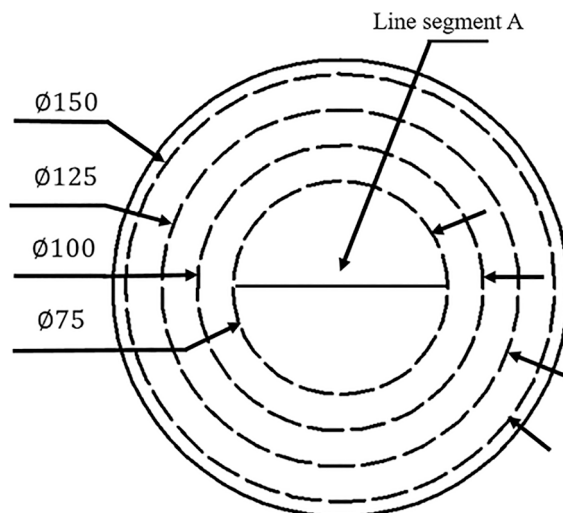


Fig. 11. Local paths for thermal comparison.

Table 4

Average temperature values on the circular paths.

Radius (mm)	Temperature (°C)		Difference w.r.t. experimental values (%)
	Numerical	Experimental	
75	346.7	346.8	0.03
100	303.6	317.7	4.44
125	260.8	292.2	10.75
150	242.3	272.2	12.98

recorded experimentally. There are two potential reasons for this difference in temperature. The first reason is the geometrical variations in the manufacturing of the gas stove. While the gas stove has been numerically modelled as a perfectly symmetrical body with accurate geometric dimensions, the same is not possible during its manufacturing due to the deviations caused during the machining processes. The diameter of outer rings fuel outlets of the gas stove is slightly bigger than the numerical model. This causes slightly higher gaseous fuel ejection from the outer rings in hot-state tests. Therefore, the experimentally measured temperature is higher than the numerically predicted temperature, especially when the radius increases. This leads to non-uniformities in the thermal characteristics of the gas stove, as evident in Fig. 10. The second reason for this difference is that in the numerical solver, the heat transfer from the quartz plate to the ambient air takes place in the horizontal direction only, whereas during the experiment, the heat transfer to the ambient air can take place in any direction. Therefore, the heat transfer in the vertical direction is prominent, resulting in the experimental temperature values being higher than numerically predicted temperature.

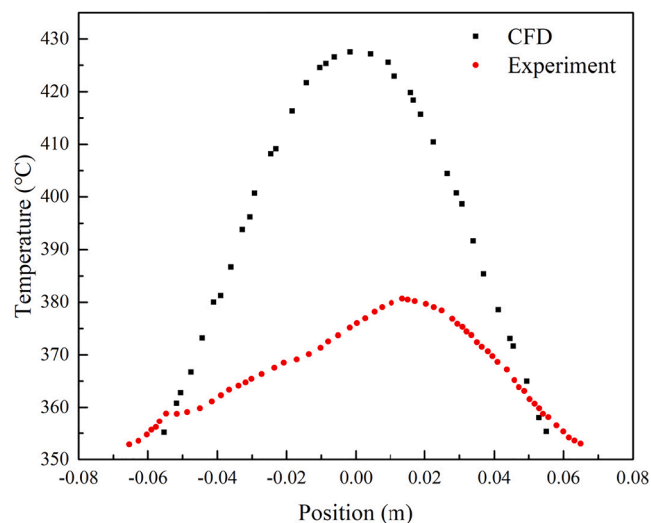
These temperature differences between the experimental and numerical models are within an acceptable range (<15 %) [41–43] and thus, the accuracy of the numerical solver employed in this study is verified.

Further analyzing the temperature differences between the experimental and numerical investigations, focusing on the region directly above the burner/rings of the swirl gas stove, temperature values have been recorded on the line segment A shown in Fig. 11. The length of this line is 150 mm and it passes through the center of the quartz plate. It can be seen in Fig. 12(a) that the maximum temperature recorded experimentally is ~380 °C, while the maximum temperature recorded numerically is ~427 °C. Thus, the difference in the maximum temperature values is ~47 °C (or ~12 %), which is consistent with the maximum temperature difference summarized in Table 4. Moreover, Fig. 12(b) depicts the deviation in experimentally and numerically recorded temperature.

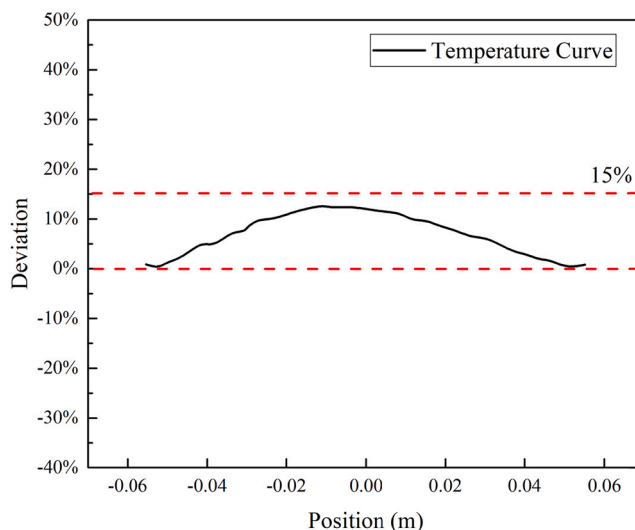
Based on these results, it can be concluded that the numerical methodology adopted in this study is capable of predicting thermal variations associated with the combustion of gases in a swirl gas stove with reasonable accuracy, and thus, it can be used for conducting thermal analysis for the combustion of hybrid methane-hydrogen mixture.

4. Numerical combustion analysis of hybrid methane-hydrogen mixture in a swirl gas stove

It is a well-known fact that hydrogen is a highly flammable and explosive gas having NFPA 704s highest rating of 4 (NFPA: National Fire Protection Association). Thus, great attention should be paid towards safety when considering hydrogen for combustion purposes. Wu [44] has stated that the explosion limit of hydrogen concentration in air is 4 % by volume i.e. <4 % hydrogen can be mixed in air for ignition and complete combustion. Similarly, the required volumetric ratio of methane in air for complete combustion is 1:10 i.e. the concentration of methane in combustion supporting air is 10 %. When hybrid methane-hydrogen is to be used for combustion purposes, the mixing ratio of



(a)



(b)

Fig. 12. (a) Local temperature variations on line segment A (b) Deviation between experimental and numerical local temperature measurements.

hydrogen can be upto 40 %. Combining the aforementioned statistics, it can be concluded that when hybrid methane-hydrogen mixture is to be used with combustion supporting air, the volumetric concentration of hydrogen cannot be >4 %.

Based on the calculation of interchangeability between methane and hydrogen, under the condition of meeting the high Wobbe number and combustion potential of natural gas, the maximum volumetric concentration of hydrogen in natural gas cannot be >23 %. Zhao et al. [10] have found through experimental investigations that backfire and deflagration will occur when hydrogen, with a volume fraction of 20 %, is added to the natural gas. Considering the safety aspects of hydrogen combustion, the numerical modelling carried out in the present study does not exceed hydrogen concentration of 15 %; the numerical investigations have been carried out on hybrid methane-hydrogen mixture, where the volume fraction of hydrogen is 5 %, 10 % and 15 % respectively. The numerical results of these investigations are discussed in the sections below.

4.1. Thermal analysis

Wind gate controlling has been adopted to ensure that the excess air coefficient remains unchanged under different hydrogen concentrations. Fig. 13 depicts the variations in total temperature within the flow domain for different concentrations of hydrogen (0 % to 15 %). It can be seen that as the concentration of hydrogen increases, the maximum temperature of the flame gradually decreases.

In order to carry out quantitative thermal analysis, thermal profiles are drawn at the outlet of fire holes shown in Fig. 13. Fig. 14 depicts that the temperature at the exit of fire holes ($x = -0.05 \text{ m}$, 0 m and 0.05 m) is high, as expected, while the temperature in the gap regions between the fire holes is relatively lower. Moreover, the temperature away from the fire holes is significantly lower. This is true for all the different concentrations of hydrogen considered in the present study. It can also be seen that as the volumetric concentration of hydrogen in methane increases, the maximum temperature at the exit of the fire holes decreases. Table 5 summarizes the maximum temperature data taken from Fig. 14. It can be seen that when 5 % hydrogen is added to methane, the maximum temperature at the exit of the fire holes decreases by 1.5 %. Further increasing hydrogen's volumetric concentration to 10 % decreases the maximum temperature by further 1.5 %, and when hydrogen's concentration reaches 15 %, there is a further $\sim 1.5 \%$ decrease in maximum temperature. Thus, it can be concluded that every 5 % increase in the volumetric concentration of hydrogen decreases the maximum temperature by 1.5.

The question arises that why the combustion temperature decreases when methane is doped with hydrogen. The low calorific values of methane and hydrogen are $\sim 35.81 \text{ MJ/m}^3$ and $\sim 10.78 \text{ MJ/m}^3$ respectively. Thus, the combustion of low calorific value hydrogen gas results in lowering the overall temperature of combustion. More the concentration of hydrogen in methane, lower the calorific value of the mixture, because hydrogen is added to the mixture in volume proportion. The molecular weight, density and mass of hydrogen is less than that of methane. The overall density and calorific value of the mixed fuel are less than those of pure methane. The volume average temperature in the flow domain for 0 %, 5 %, 10 % and 15 % hydrogen concentrations have been computed to be 886 K, 875 K, 857 K and 827 K respectively. In comparison with the volume average temperature of pure methane, the temperature in the flow domain decreases by 1.2 % (5 % H_2), 3.3 % (10

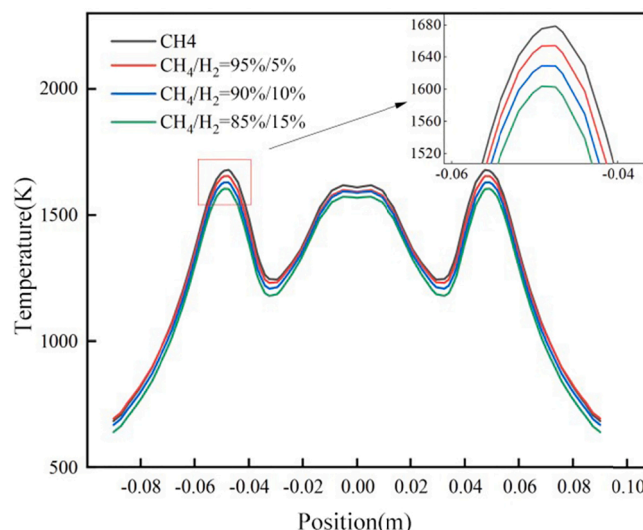


Fig. 14. Temperature distribution at the exit of fire holes for different concentrations of hydrogen.

Table 5
Maximum temperature variations.

Hydrogen Concentration (%)	Maximum Temperature (K)	Difference w.r.t. 0 % concentration (%)
0	1680	–
5	1655	1.5
10	1629	3.0
15	1603	4.6

% H_2) and 6.7 % (15 % H_2) respectively. It is noteworthy here that although the percentage decrease in maximum temperature at the fire holes' outlets has been observed to be constant with increasing hydrogen concentration, the percentage decrease in average temperature in the flow domain increases.

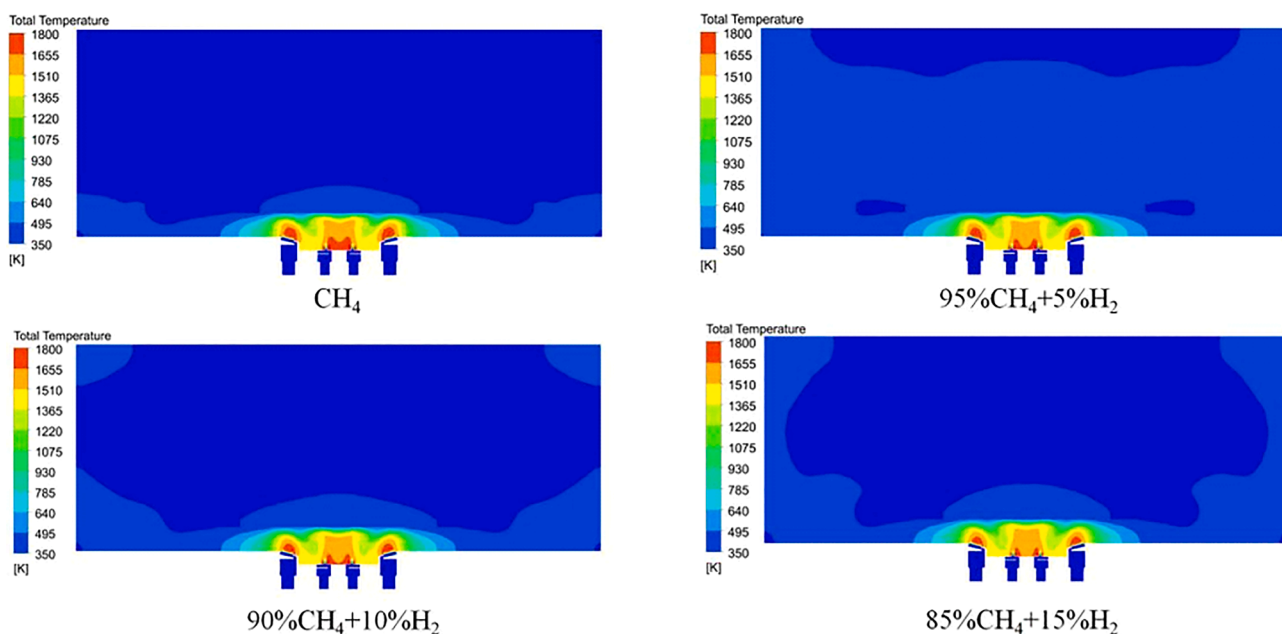


Fig. 13. Total temperature variations for different volumetric concentrations of hydrogen.

4.2. Combustion products analysis

When a carbonaceous fuel is burned incompletely, CO is produced, which has serious health risks for humans as it is highly toxic gas which is colorless and odorless. The production of CO is considerably affected by the combustion temperature; lower combustion temperature leads to more production of CO [45]. It has been observed in the previous section that hybrid methane-hydrogen mixture results in lower combustion temperature. This has the potential to produce more CO. However, at the same time, hydrogen is not a carbonaceous gas, thus the combustion of hydrogen cannot lead to any carbon gases. There is a need to carry out a detailed analysis on the combustion products from hybrid methane-hydrogen mixture in order to find out whether this mixture results in more or lower CO production.

Fig. 15 depicts the variations in CO mole fraction for different hydrogen concentrations under consideration (i.e. 0 %, 5 %, 10 % and 15 %). It can be clearly seen that the CO production from pure methane combustion is high, as expected, and thus, higher CO mole fraction distribution is evident under the heat-resistant quartz plate, from where CO then disperses radially outwards into the ambient air. As the volumetric concentration of hydrogen increases, significant decrease in CO production can be noticed. In order to quantify the variations in CO produced from different concentrations of hydrogen, Fig. 16 shows the distribution of CO mole fraction at the exit of fire holes.

It can be seen in Fig. 16 that the mole fraction of CO remains almost constant at the exit of fire holes however, as the concentration of hydrogen increases, a significant decrease in CO production is observed. For pure methane combustion, the mole fraction of CO is ~ 0.083 , which decreases to 0.074, 0.069 and 0.062 as hydrogen concentration increases to 5 %, 10 % and 15 % respectively. Thus, the decrease in CO mole fraction is 11 % (5 % H₂), 17 % (10 % H₂) and 25 % (15 % H₂).

The decrease in CO production from hydrogen doped methane is related to the products of combustion reactions of methane and hydrogen. Generally speaking, the reaction path of methane is $\text{CH}_4 \rightarrow \text{CH}_3 \rightarrow \text{CH}_2\text{O} \rightarrow \text{HCO} \rightarrow \text{CO} \rightarrow \text{CO}_2$, while the reaction path of hydrogen is $\text{H}_2 \rightarrow \text{HO}_2/\text{H} \rightarrow \text{OH} \rightarrow \text{H}_2\text{O}$. Hydrogen reacts earlier and more violently than methane, which improves the temperature of methane reaction. Since the minimum ignition energy of hydrogen is 6 % of that of natural gas, hydrogen is easy to ignite and starts the chemical reaction

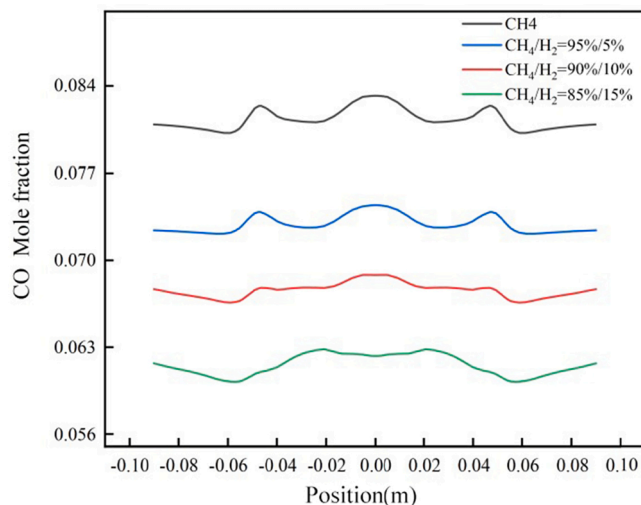


Fig. 16. CO mole fraction distribution at the exit of fire holes for different concentrations of hydrogen.

before natural gas. After being ignited, hydrogen provides energy for the ignition of natural gas, so the ignition temperature (initial reaction temperature) of the mixture composed of natural gas and hydrogen increases. Therefore, adding hydrogen to methane can effectively reduce the production of CO. The average concentrations of CO within the flow domain, resulting from the combustion of hybrid methane-hydrogen mixture, is shown in Fig. 17. It can be seen that as the concentration of hydrogen increases, the average concentration of CO in the flow domain decreases. This decrease in CO mole fraction has been observed to be almost linear, which indicates that methane doped with 15 % of hydrogen (by volume) is the optimum combination for combustion in domestic swirl gas stoves.

4.3. Experimental validation of hybrid methane-hydrogen mixture combustion

In order to validate the accuracy of the numerical simulations,

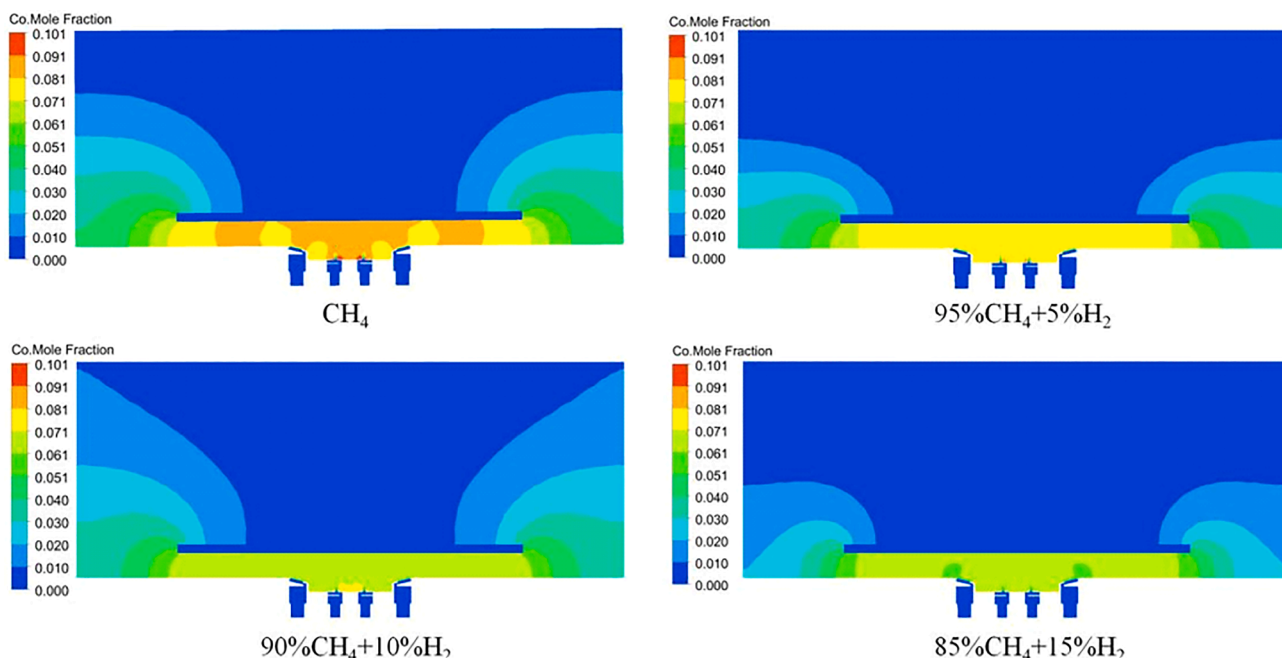


Fig. 15. CO mole fraction variations for different volumetric concentrations of hydrogen.

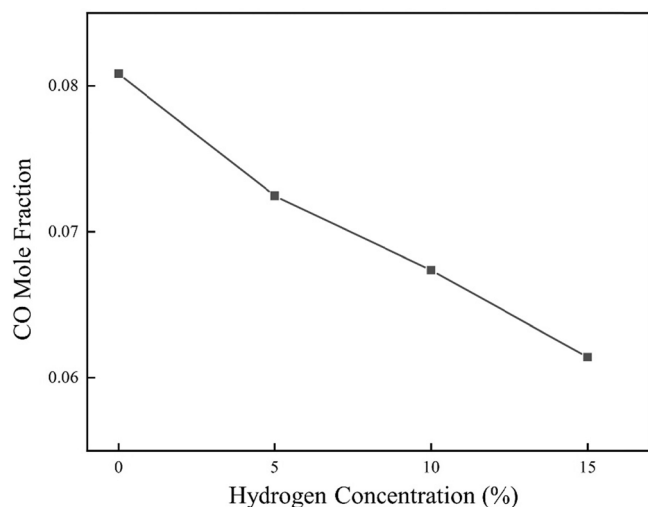


Fig. 17. Variations in average CO mole fraction within the flow domain for different hydrogen concentrations.

combustion experiments have been conducted using hybrid 85 % Methane and 15 % Hydrogen mixture. The temperature distribution and carbon monoxide emissions have been measured and compared against the numerical results in Figs. 18 and 19. It has been found that the maximum temperature difference between the two data sets is <5 %, while the maximum difference in CO mole fraction is <3 %. Thus, it is evident that the numerically predicted results for the combustion of hybrid methane-hydrogen mixture are reasonably accurate.

5. Conclusions

A simplified mechanism for the combustion of hybrid methane-hydrogen mixture has been developed based on the detailed model (GRI-Mech 3.0) using sensitivity analysis, direct relation graph and direct relation graph error propagation. The novel simplified mechanism has been implemented with a conventional numerical solver (CFD) to investigate the combustion characteristics of hybrid methane-hydrogen gas mixture in a domestic swirl gas stove, and the results for temperature and CO mole fraction have been validated against hot-state test data. The main conclusions that can be drawn based on the results obtained are:

1. The simplified mechanism reduces the number of chemical reactions by 82 % compared to the conventional detailed mechanism, thus significantly reducing computational power requirements, while maintaining an accuracy of >99 %.
2. For methane only combustion, the maximum difference between the numerical results and the experimental data is <15 %, demonstrating the usefulness of the simplified mechanism.
3. For the combustion of hybrid methane-hydrogen mixture, the maximum difference between numerical and experimental data sets is <5 %, while the maximum difference in CO mole fraction is <3 %.
4. When methane is mixed with 15 % hydrogen by volumetric concentration, CO emission reduces by 25 %, while the combustion zone's average temperature reduces by 6.7 %.
5. For 15 % Hydrogen doped natural gas, the difference between numerically predicted and experimentally recorded temperature and CO mole fraction is <5 % and <3 % respectively, clearly demonstrating the accuracy of the simplified mechanism developed.

In this study, Hydrogen concentration of upto 15 % has been investigated. The influence of other mixing ratios of hydrogen (including mass ratio) on mixed fuel combustion has not been investigated. These investigations will become part of our follow-up research work.

Funding

This research did not receive any specific grant from funding agencies in the public, commercial, or not-for-profit sectors.

CRediT authorship contribution statement

Xiaozhou Liu: Conceptualization, Methodology, Validation, Writing – original draft, Supervision, Project administration. **Guangyu Zhu:** Conceptualization, Methodology, Validation, Formal analysis, Data curation, Writing – original draft. **Taimoor Asim:** Validation, Investigation, Writing – review & editing. **Rakesh Mishra:** Investigation, Writing – review & editing.

Declaration of Competing Interest

The authors declare that they have no known competing financial interests or personal relationships that could have appeared to influence the work reported in this paper.

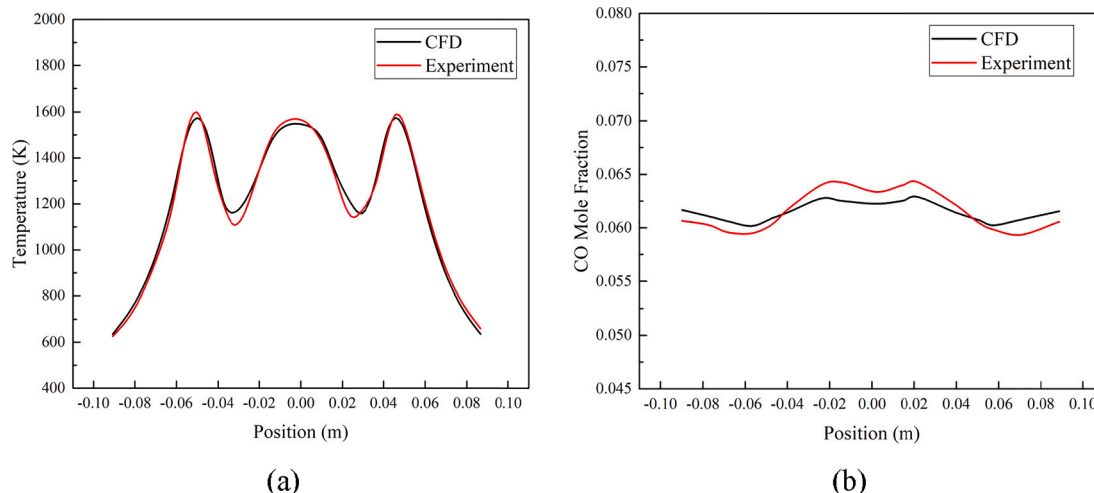


Fig. 18. Variations in (a) Temperature and (b) CO mole fraction for 15 % hydrogen concentration.

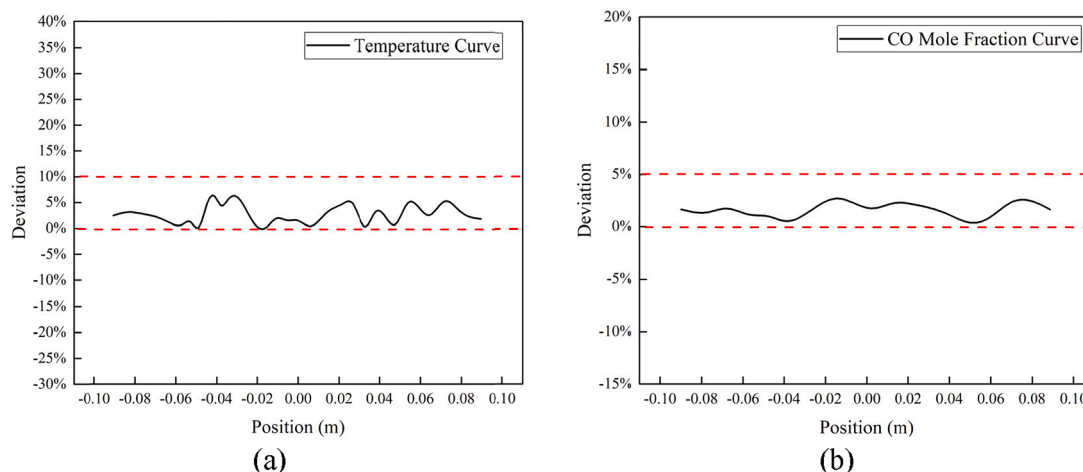


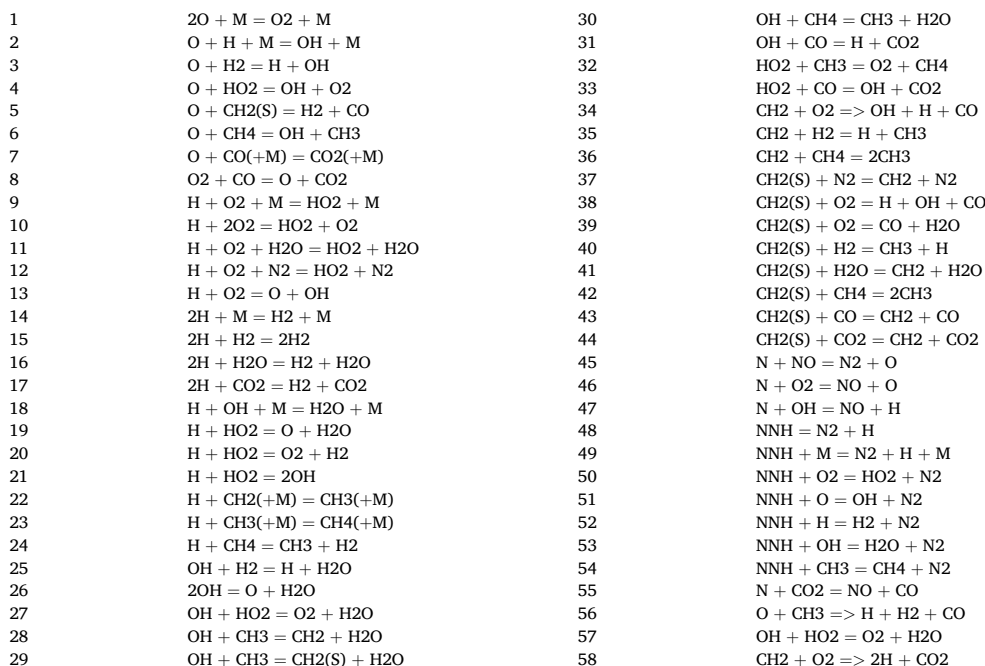
Fig. 19. Deviation between experimental and numerical (a) temperature and (b) CO mole fraction measurements.

Data availability

The data that has been used is confidential.

Appendix

Simplified reaction model.



References

- [1] Paris Agreement (2015) United Nations Framework Convention on Climate Change, T.I.A.S. 16-1104.
- [2] British Petroleum report (2021) Statistical Review of World Energy, 70th edition, 2021.
- [3] Zhang SH, Peng X, Yan LF. Smoke pollutants of domestic natural gas stoves under different flame combustion conditions. *Chemical Progress* 2012;234-8.
- [4] Haeseldonckx D, D'haeseleer W. The use of the natural-gas pipeline infrastructure for hydrogen transport in a changing market structure. *Int J Hydrogen Energy* 2007;32:1381-6.
- [5] Hu E, Huang Z, (2009) He J, et al. Experimental and numerical study on laminar burning characteristics of premixed methane-hydrogen-air flames, *International Journal of Hydrogen Energy* 34(11) 4876-4888.
- [6] Donohoe N, Heufer A, Metcalfe WK, et al. Ignition delay times, laminar flame speeds, and mechanism validation for natural gas/hydrogen blends at elevated pressures. *Combust Flame* 2014;161(6):1432-43.
- [7] Ahmed AM, Desgroux P, Gasnot L, et al. Experimental and numerical study of rich methane/hydrogen/air laminar premixed flames at atmospheric pressure:

- influence of hydrogen addition on soot precursors. *Int J Hydrogen Energy* 2016;41(16):6929–42.
- [8] Ying Y, Liu D. Detailed influences of chemical effects of hydrogen as fuel additive on methane flame. *Int J Hydrogen Energy* 2015;40(9):3777–88.
- [9] Luo ZX, Xu HC, Yuan M. Test and evaluation of the safety and emission performance of the combustion of natural gas mixed with hydrogen on domestic gas appliances. *Oil and Gas Chemical Industry* 2019;48:50–6.
- [10] Zhao Y, Vincent M, Samuelsen S. Influence of hydrogen addition to pipeline natural gas on the combustion performance of a cooktop burner. *Int J Hydrogen Energy* 2019;44:12239–53.
- [11] Jiang SJL, Zhang ZJ, C. Numerical simulation research on swirl gas stove. *Thermal Sci Technol* 2009;8:337–42.
- [12] Chen L, Feng L, Peng W. Numerical simulation of high-power domestic gas stove. *Shanghai Gas* 2020;1:4.
- [13] Pashchenko D. Hydrogen-rich fuel combustion in a swirling flame: CFD-modeling with experimental verification. *Int J Hydrogen Energy* 2020;45:19996–20003.
- [14] Sun M, Huang X, Hu Y. Effects on the performance of domestic gas appliances operated on natural gas mixed with hydrogen. *Energy* 2022;244:122557.
- [15] Jones DR, Al-Masry WA, Dunnill C. Hydrogen-enriched natural gas as a domestic fuel: an analysis based on flash-back and blow-off limits for domestic natural gas appliances within the UK. *Sustainable Energy Fuels* 2018;2:710–23.
- [16] Zhao Y, McDonell V, Samuelsen S. Experimental assessment of the combustion performance of an oven burner operated on pipeline natural gas mixed with hydrogen. *Int J Hydrogen Energy* 2019;44:26049–62.
- [17] Gimeno-Escobedo E, Cubero A, Ochoa JS. A reduced mechanism for the prediction of methane-hydrogen flames in cooktop burners. *Int J Hydrogen Energy* 2019;44:27123–40.
- [18] Hou JL, Jin P, Cai GB. Simplified mechanism of oxygen/methane combustion reaction based on sensitivity analysis. *Aerodyn J* 2012;27:1549–54.
- [19] Jiang B, Ji Q, Zhao CP. Simplification mechanism of methane/air combustion and its application. *J Henan Univ Sci Technol* 2016;37:24–8.
- [20] Wang LY, Wang ZF, Chen WH. Simplified detailed chemical reaction mechanism of high-temperature combustion of phenolic resin pyrolysis products. *J Nanjing Univ Aeronaut Astronaut* 2020;52:131–41.
- [21] Ruan D, Qi YY, Li HD. Numerical simulation study of NO reduction by CO at high temperature without catalyst. *Silicate J* 2016;35:1674–81.
- [22] Lu TF, Law CK. A directed relation graph method for mechanism reduction. *Proc Combust Inst* 2005;30:1333–41.
- [23] Fany YM, Wany QD, Wany F, Li XY. Reduction of the Detailed Kinetic mechanism for high-temperature combustion of n-dodecane. *Acta Physico-Chimica Sinica* 2012;28: 2536–2542(7).
- [24] Lu T, Law CK. Linear time reduction of large kinetic mechanisms with directed relation graph: n-Heptane and iso-octane. *Combust Flame* 2006;144:24–36.
- [25] Poon H, Ng H, Gan S, Pang K. Evaluation and development of chemical kinetic mechanism reduction scheme for biodiesel and diesel fuel surrogates. *SAE Int J Fuels Lubr* 2013;6:729–44.
- [26] Monnier F, Ribert G. Simulation of high-pressure methane-oxygen combustion with a new reduced chemical mechanism. *Combust Flame* 2022;235:111735.
- [27] Niemeyer KE, Sung C, Raju MP. Skeletal mechanism generation for surrogate fuels using directed relation graph with error propagation and sensitivity analysis. *Combust Flame* 2010;157:1760–70.
- [28] Tang A, Huang Q, Li Y. Development and verification of simplified methane/dimethyl ether mechanism for micro-combustion. *Fuel Process Technol* 2022;226: 107071.
- [29] Zheng XL, Lu TF, Law CK. Experimental counterflow ignition temperatures and reaction mechanisms of 1, 3-butadiene. *Proc Combust Inst* 2007;31:367–75.
- [30] Hu F, Li P, Guo J. Evaluation, development, and validation of a new reduced mechanism for methane oxy-fuel combustion. *Int J Greenhouse Gas Control* 2018; 78:327–40.
- [31] Li R, Konnov AA, He G. Chemical mechanism development and reduction for combustion of NH₃/H₂/CH₄ mixtures. *Fuel* 2019;257:116059.
- [32] CHEMKIN 10112 (2011) *Reaction Design: San Diego, USA*.
- [33] Glarborg P, Kee RJ, Grcar JF. *PSR: A FORTRAN program for modeling well stirred reactors*. CA, USA: Sandia National Laboratories Livermore; 1986.
- [34] Luo DD, Zhen HS, Leung CW. Premixed flame impingement heat transfer with induced swirl. *Int J Heat Mass Transf* 2010;53:4333–6.
- [35] ANSYS, Inc. (2022) *ANSYS Fluent User's Guide, Release 22R1*.
- [36] Singh D, Aliyu AM, Charlton M, Mishra R, Asim T, Oliveira AC. Local multiphase flow characteristics of a severe-service control valve. *J Petrol Sci Eng* 2020;195: 107557.
- [37] Asim, T, Mishra, R, Kaysthaqir, S. and Aboufares, G. (2015) Performance Comparison of a Vertical Axis Wind Turbine using Commercial and Open-Source Computational Fluid Dynamics based Codes; In the proceedings of the International Conference on Jets, Wakes and Separated Flows, Stockholm, Sweden.
- [38] Hindasageri V, Kuntikana P, Vedula RP, Prabhui SV. An experimental and numerical investigation of heat transfer distribution of perforated plate burner flames impinging on a flat plate. *Int J Therm Sci* 2015;94:156–69.
- [39] Zheng HF. *Analysis of Heat Loss of Gas Stove and Efficient Gas stove*. China: Huazhong University of Science & Technology; 2018.
- [40] Jin L, Zhou JS, Wu YM. Research on gasification performance of downdraft biomass gasifier. *Thermal Power Eng* 2011;26:105–9.
- [41] Galletti C, Giovanni C, Leonardo T. Numerical investigation of oxy-natural-gas combustion in a semi-industrial furnace: validation of CFD sub-models. *Fuel* 2013; 109:445–60.
- [42] Su Y, Chen C, Su A. Simulation of high temperature air combustion with modified eddy-break-up combustion model. *Energy Procedia* 2012;14:127–32.
- [43] Yin C. Prediction of air-fuel and oxy-fuel combustion through a generic gas radiation property model. *Appl Energy* 2017;189:449–59.
- [44] Wu C. Feasibility study on blending hydrogen into natural gas distribution networks. China: Chongqing University; 2018.
- [45] Craig M, Asim T. Numerical investigations on the propagation of fire in a railway carriage. *Energies* 2020;13:4999.